IgD class switching is initiated by microbiota and limited to mucosa-associated lymphoid tissue in mice

Jin Huk Choi[a], Kuan-wen Wang[a], Duanwu Zhang[a], Xiaowei Zhan[a,b], Tao Wang[a,b], Chun-Hui Bu[a], Cassie L. Behrendt[c,d], Ming Zeng[a], Ying Wang[a], Takuma Misawa[a], Xiaohong Li[a], Miao Tang[a], Xiaoming Zhan[a], Lindsay Scott[a], Sara Hildebrand[a], Anne R. Murray[a], Eva Marie Y. Moresco[a], Lora V. Hooper[c,d], and Bruce Beutler[a,1]

[a]Center for the Genetics of Host Defense, University of Texas Southwestern Medical Center, Dallas, TX 75390; [b]Quantitative Biomedical Research Center, Department of Clinical Science, University of Texas Southwestern Medical Center, Dallas, TX 75390; [c]Department of Immunology, University of Texas Southwestern Medical Center, Dallas, TX 75390; and [d]Howard Hughes Medical Institute, University of Texas Southwestern Medical Center, Dallas, TX 75390

Contributed by Bruce Beutler, December 28, 2016 (sent for review December 11, 2016; reviewed by David Nemazee and David J. Rawlings)

Class-switch recombination (CSR) alters the Ig isotype to diversify antibody effector functions. IgD CSR is a rare event, and its regulation is poorly understood. We report that deficiency of 53BP1, a DNA damage-response protein, caused age-dependent overproduction of secreted IgD resulting from increased IgD CSR exclusively within B cells of mucosa-associated lymphoid tissues. IgD overproduction was dependent on activation-induced cytidine deaminase, hematopoietic MyD88 expression, and an intact microbiome, against which circulating IgD, but not IgM, was reactive. IgD CSR occurred via both alternative nonhomologous end-joining and homologous recombination pathways. Microbiota-dependent IgD CSR also was detected in nasal-associated lymphoid tissue of WT mice. These results identify a pathway, present in WT mice and hyperactivated in 53BP1-deficient mice, by which microbiota signal via Toll-like receptors to elicit IgD CSR.

IgD | class-switch recombination | 53BP1 | microbiota | Toll-like receptor

Derived from a single alternatively spliced transcript, IgM and IgD share antigenic specificity and are expressed simultaneously by antigen-naïve mature B cells. After activation by antigen, B cells undergo classical class-switch recombination (cCSR) mediated by DNA-editing enzymes and DNA double-strand break (DSB) repair proteins, in which the *Igh* Cμ or δ exon is replaced with Cγ, Cε, or Cα, altering the Ig isotype. Less frequently, activated B cells undergo class switching to IgD, which occurs through recombination targeting the switch region preceding Cμ (Sμ) and a noncanonical switch-like region 5′ to Cδ known as σ_δ.

The regulation of IgD CSR clearly differs from that of cCSR (1), and the biological importance of IgD, which is functionally redundant with IgM in several processes (2, 3), has not been fully elucidated. Here we report the investigation of a hyper-IgD syndrome caused by deficiency of the DNA damage-response protein p53-binding protein 1 (53BP1), which revealed previously unknown fundamental characteristics of IgD CSR, including confinement to defined anatomic sites and dependence on TLR-activating signals from the microbiome.

Results

B-Cell–Intrinsic Age-Dependent Hyper-IgD Syndrome Caused by a *Trp53bp1* Mutation. To identify the genes involved in lymphopoiesis, we carried out a forward genetic screen in mice carrying *N*-ethyl-*N*-nitrosourea (ENU)-induced mutations. We screened 49,825 G3 mice derived from 1,725 G1 grandsires bearing 90,151 nonsynonymous mutations within the coding regions or splice junctions of 19,913 genes. A total of 66,681 mutations in 16,061 genes were tested three or more times in the homozygous state; these included one or more putative null alleles of 5,300 genes. Among the phenovariants discovered, several mice in two of three ancestrally related pedigrees exhibited low surface IgD expression on peripheral blood B cells compared with wild-type (WT) mice (Fig. 1 *A* and *B*, *Inset*). The phenotype, named *lentil*, was transmitted as a recessive trait.

By superpedigree mapping, a method that analyzes genotype vs. phenotype associations from multiple combined pedigrees with identical or nonidentical allelic mutations (4), the *lentil* phenotype was correlated with a mutation in *Trp53bp1* encoding transformation-related 53BP1, a DNA damage-response protein (Fig. 1*B*). The *lentil* mutation, present in the affected pedigrees, was predicted to impair the splicing of exon 8, resulting in a frameshift and premature termination; significantly reduced 53BP1 protein expression was detected in homozygous *lentil* mutants (Fig. S1). Point mutations in phospholipase A2, group IVB (*Pla2g4b*) and G protein-coupled receptor 176 (*Gpr176*) also scored in the mapping of the *lentil* phenotype (Fig. 1*B*). Mice expressing a CRISPR/Cas9-targeted null allele of *Trp53bp1*, but not of *Pla2gb4*, recapitulated the *lentil* phenotype, confirming the *Trp53bp1* mutation as causative (Fig. 1*C*).

The reduction in surface IgD expression on peripheral B cells of *Trp53bp1*$^{-/-}$ mice was strongly age-dependent, occurring progressively after 6 wk of age (Fig. 1*D*). B cells in the bone marrow (BM), spleen, and peritoneal cavity of *Trp53bp1*$^{-/-}$ mice showed no significant differences in surface IgD and IgM expression compared with WT littermates (Fig. S2 *A*–*C*). These findings are consistent with a previous report of normal IgM and IgD expression on B cells from the spleen and lymph nodes of mice with a different null allele of *Trp53bp1* (5). Notably, we observed reduced mean fluorescence intensity (MFI) of IgD immunostaining on *Trp53bp*$^{-/-}$ peripheral blood B cells only when immunostaining was performed in the presence of serum (Fig. 1*E*); moreover, reduced IgD MFI was

Significance

Immunoglobulins exist in several forms, or isotypes, that carry out distinct effector functions. During an antibody response, B cells can switch their immunoglobulin isotype through the process of class-switch recombination (CSR). CSR to IgD is a rare event compared with CSR to other isotypes, and its regulation is poorly understood. Here we report that mice lacking the DNA damage-response protein 53BP1 display a hyper-IgD syndrome despite deficiencies of other immunoglobulin classes. By studying these mice, we discovered that CSR to IgD in 53BP1 mutant mice and in wild-type mice depends on an intact microbiome and Toll-like receptor signaling, and is anatomically confined to B cells of mucosa-associated lymphoid tissues.

Author contributions: J.H.C. and B.B. designed research; J.H.C., K.-w.W., D.Z., C.L.B., M.Z., Y.W., T.M., X.L., M.T., Xiaoming Zhan, and L.S. performed research; Xiaowei Zhan, T.W., C.-H.B., and L.V.H. contributed new reagents/analytic tools; J.H.C., S.H., and B.B. analyzed data; and J.H.C., A.R.M., E.M.Y.M., and B.B. wrote the paper.

Reviewers: D.N., The Scripps Research Institute; and D.J.R., Children's Hospital and Regional Medical Center.

The authors declare no conflict of interest.

[1]To whom correspondence should be addressed. Email: Bruce.Beutler@UTSouthwestern.edu.

This article contains supporting information online at www.pnas.org/lookup/suppl/doi:10.1073/pnas.1621258114/-/DCSupplemental.

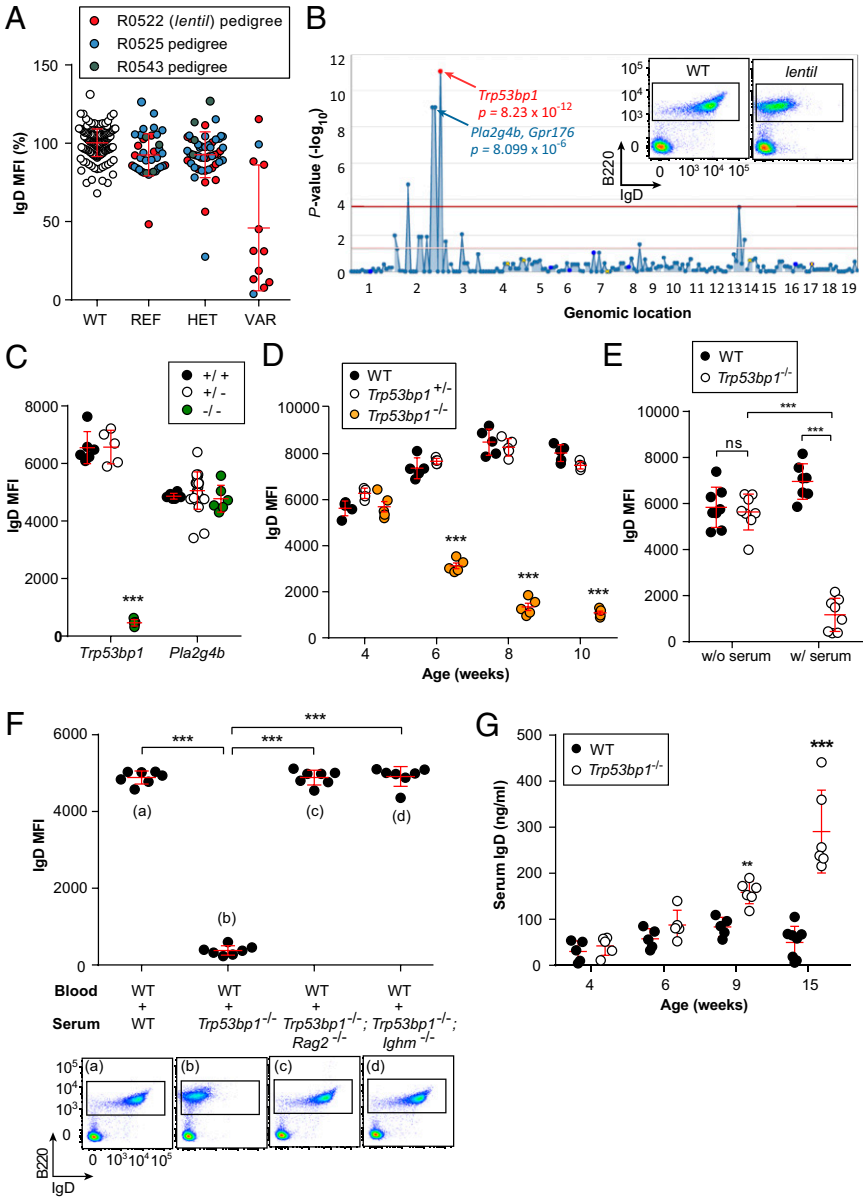

Fig. 1. Age-dependent hyper-IgD syndrome caused by an ENU-induced *Trp53bp1* mutation in mice. (*A*) MFI of surface IgD immunostaining (IgD MFI) on peripheral blood B cells from WT C57BL/6J mice (WT), or from three pedigrees of third generation (G3) descendants of a single ENU-mutagenized male mouse, with REF ($^{+/+}$), HET (*+/lentil*), or VAR (*lentil/lentil*) genotypes for *Trp53bp1*. Data were normalized to average IgD MFI of age matched C57BL/6 mice at the time of experiment. (*B*) Manhattan plot. $-\text{Log}_{10}$ *P* values plotted vs. the chromosomal positions of mutations identified in the three G1 founders of the affected pedigrees. (*Insets*) Representative flow cytometry analysis of IgD expression by peripheral blood B cells from a homozygous *lentil* mouse and a WT littermate. (*C*) IgD MFI on peripheral blood B cells from 12-wk-old *Trp53bp1*$^{-/-}$ or *Pla2g4b*$^{-/-}$ mice generated by the CRISPR/Cas9 system. (*D*) IgD MFI on peripheral blood B cells from mice of the indicated ages and genotypes. Cells were stained in the presence of serum. (*E*) IgD MFI on peripheral blood B cells from 12-wk-old *Trp53bp1*$^{-/-}$ and WT littermates; cells were stained in the presence or absence of serum. (*F*) IgD MFI on WT peripheral blood B cells after immunostaining in the presence of serum from the indicated mouse strains. (*Insets*) Representative flow cytometry analysis of IgD expression under each serum condition. (*G*) Serum IgD concentration in mice of the indicated ages and genotypes. In *A* and *C*–*G*, data points represent individual mice. In *C*–*G*, *P* values were determined by Student's *t* test, and unless indicated otherwise correspond to differences between the marked group and WT. Results are representative of two to three independent experiments with $n = 5$–23 mice/genotype or strain; error bars indicate SD.

detected on WT B cells stained in the presence of serum from *Trp53bp1*$^{-/-}$ mice, but not from WT, *Trp53bp1*$^{-/-}$;*Rag2*$^{-/-}$, or *Trp53bp1*$^{-/-}$;*Ighm*$^{-/-}$ mice (Fig. 1*F*). These findings suggest that soluble factor(s) secreted by *Trp53bp1*-deficient B cells decrease IgD expression on B cells.

In agreement with previous reports, we confirmed that *Trp53bp1*-deficient mice lacked *Igh* cCSR (Fig. S2*D*). Surprisingly, the *Trp53bp1*$^{-/-}$ mice exhibited a progressive age-dependent increase in serum IgD (Fig. 1*G*). This phenotype was confirmed in mixed BM chimeras (Fig. S3). These results led us to reinterpret the apparently low IgD MFI in *Trp53bp1*$^{-/-}$ peripheral blood B cells. We concluded that age-dependent reduction in IgD MFI on peripheral blood B cells corresponds to neutralization of the fluorescent-labeled IgD antibody by excess serum IgD; thus, *Trp53bp1*$^{-/-}$ mice have a hyper-IgD phenotype.

Active IgD CSR in *Trp53bp1*$^{-/-}$ Mice Occurs in Mucosa-Associated Lymphoid Tissue. Aside from a mevalonate kinase (MvK) or IgH 3′ regulatory region (3′RR) deficiency (1, 6–8), no other molecular causes of hyper-IgD syndrome have been established

to date. The hyper-IgD phenotype observed in the *Trp53bp1*$^{-/-}$ mice was not seen in other immunodeficiency states, including those in mice homozygous for null alleles of *Tnfsf13b*, *Cd40*, *Dock8, Aicda*, or *Atm* (Fig. 2 *A* and *B*). Thus, we sought to understand the special function of 53BP1 in the regulation of IgD production.

Secreted IgD is produced either from alternative splicing of pre-mRNA encompassing C_μ and C_δ exons or from S_μ-σ_δ CSR, a process that requires activation-induced cytidine deaminase (AID) (9). Quantitative RT-PCR analysis of I_μ-C_δ and I_μ-C_μ transcripts verified that excessive alternative splicing to produce I_μ-C_δ transcripts did not occur in *Trp53bp1*$^{-/-}$ B cells (Fig. S4 *A* and *B*). To determine whether the hyper-IgD phenotype in *Trp53bp1*$^{-/-}$ B cells is associated with increased S_μ-σ_δ CSR events, we created *Trp53bp1*$^{-/-}$;*Aicda*$^{-/-}$ mice using the CRISPR/Cas9 system. AID deficiency completely suppressed the hyper-IgD phenotype of the *Trp53bp1*$^{-/-}$ mice (Fig. 2 *C* and *D*).

We isolated B cells from primary and secondary lymphoid tissues, including those associated with mucosa that contact commensal microbes, and performed Southern blot analysis of S_μ-σ_δ junctions using a 5′ C_δ probe (Fig. S4*C*) to determine the localization of B cells undergoing IgD CSR. We found that extensive S_μ-σ_δ CSR occurred in *Trp53bp1*$^{-/-}$ B cells located in nasal-associated lymphoid tissue (NALT), a subtype of mucosal-associated lymphoid tissue (MALT), in the closely localized submandibular lymph nodes (SMLNs), as well as in mesenteric lymph nodes (MLNs), which are proximate to gut-associated lymphoid tissue (another subtype of MALT) (Fig. 2*E*). This active S_μ-σ_δ CSR was abrogated in *Trp53bp1*$^{-/-}$;*Aicda*$^{-/-}$ mice (Fig. 2*E*). Taken together, these data demonstrate that 53BP1 deficiency results in a loss of cCSR with

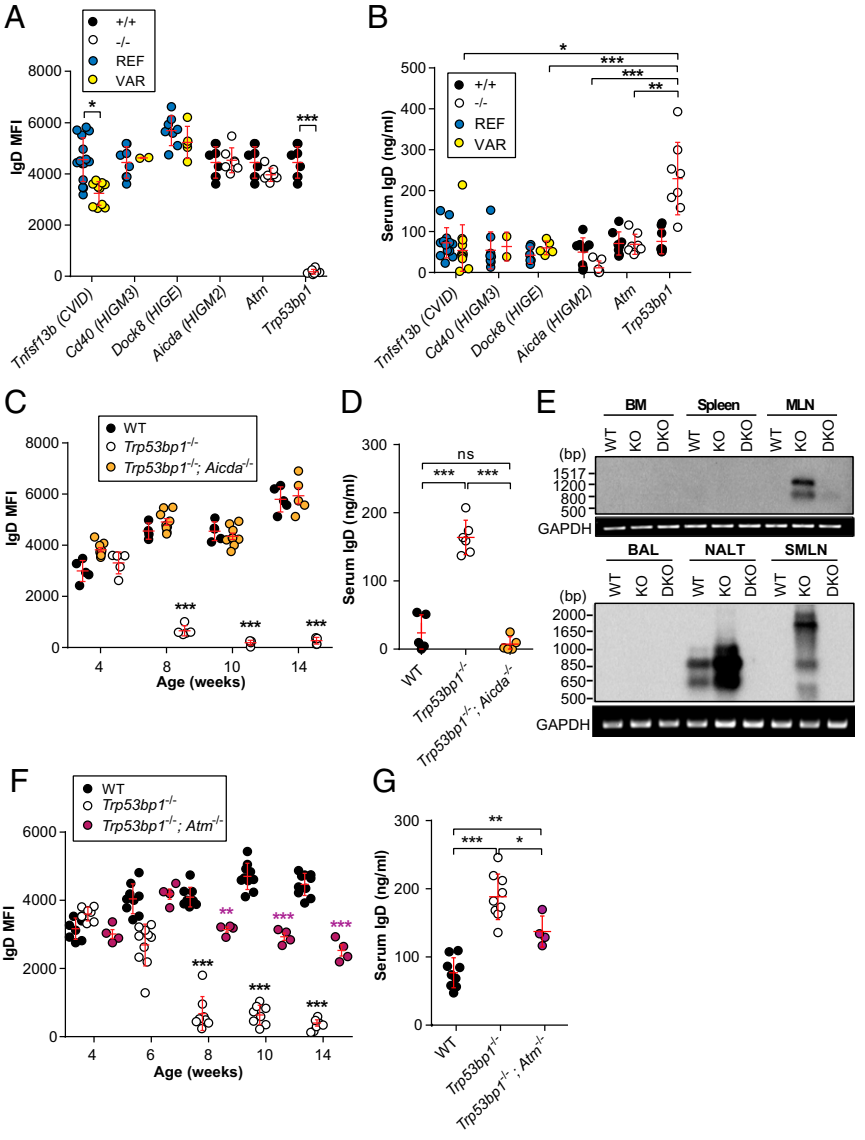

Fig. 2. *Trp53bp1*-deficient B cells of MALT undergo IgD CSR. (*A*, *C*, and *F*) IgD MFI on peripheral blood B cells from mice carrying homozygous ENU-induced mutations in *Tnfsf13b*, *Cd40*, or *Dock8*, or mice with null mutations of *Aicda*, *Atm*, *Trp53bp1*, *Trp53bp1;Aicda*, or *Trp53bp1;Atm*. REF, homozygous for the WT allele; VAR, homozygous for the mutant allele. Cells were stained in the presence of serum. (*B*, *D*, and *G*) Serum IgD concentration in 14-wk-old mice of the indicated strains or genotypes. Results are representative of two independent experiments, $n = 2$–13 mice/genotype or strain. (*E*) Southern blot analysis of S_μ-σ_δ junctions in B cells from BM, spleen, MLNs, bronchoalveolar lavage fluid (BAL), NALT (a subtype of MALT), and SMLNs of 14-wk-old *Trp53bp1*$^{-/-}$ (KO), *Trp53bp1*$^{-/-}$;*Aicda*$^{-/-}$ (DKO), and WT littermates. Results are representative of three independent experiments using pooled samples from mice of the indicated genotypes.

a concomitant increase in AID-dependent S_μ-σ_δ CSR at defined anatomic sites that more than compensates for the loss of cCSR.

In the absence of 53BP1, AID-mediated DNA DSBs at the *Igh* locus are repaired by ATM-dependent alternative nonhomologous end-joining (A-NHEJ; suppressed by canonical NHEJ) in the G1 phase or by homologous recombination (HR) in the S-G2/M phase of the cell cycle (10–13). Extensive DNA template resection in HR inhibits ATM activity and reduces the formation of chromosomal translocations via A-NHEJ (14). To gain insight into the DSB repair pathway necessary for manifestation of the hyper-IgD phenotype, we generated *Trp53bp1*$^{-/-}$;*Atm*$^{-/-}$ mice. ATM deficiency partially suppressed serum IgD levels in *Trp53bp1*$^{-/-}$ mice (Fig. 2 *F* and *G*).

S_μ-σ_δ CSR in human respiratory mucosa B cells results in generation of IgD-producing plasmablasts that secrete IgD reactive to respiratory bacteria (9). We hypothesized that secreted IgD produced by B cells of the gut mucosa of *Trp53bp1*$^{-/-}$ mice may target antigens derived from intestinal microbial flora. In a flow cytometry assay, we measured the binding of serum IgD from *Trp53bp1*$^{-/-}$ mice to intestinal bacteria isolated from *Ighm*$^{-/-}$ mice, which produce no IgM or IgD, and IgA at levels similar to those in *Rag2*$^{-/-}$ mice. We observed that secreted IgD produced by *Trp53bp1*$^{-/-}$ B cells recognized intestinal bacteria (Fig. 3*A*); in contrast, secreted IgM from WT or *Trp53bp1*$^{-/-}$ mice failed to bind intestinal bacteria. Secreted IgA from WT mice, but not from *Trp53bp1*$^{-/-}$ mice, also bound intestinal bacteria. The staining was specific for IgD, because IgD$^+$ bacteria were absent after incubation with sera from *Ighm*$^{-/-}$ and *Trp53bp1*$^{-/-}$;*Ighm*$^{-/-}$ mice or WT littermates. In vivo, the quantity of IgD-bound colonic bacteria was comparable in WT, *Ighm*$^{-/-}$, *Trp53bp1*$^{-/-}$, and *Trp53bp1*$^{-/-}$;*Ighm*$^{-/-}$ mice, but higher levels of IgD-coated small intestinal bacteria were detected in *Trp53bp1*$^{-/-}$ mice relative to WT, *Ighm*$^{-/-}$, or *Trp53bp1*$^{-/-}$;*Ighm*$^{-/-}$ mice (Fig. 3*B*). In contrast, IgA-coated intestinal bacteria were significantly decreased in *Trp53bp1*$^{-/-}$ mice compared with WT littermates (Fig. 3*C*). These data indicate that serum IgD from *Trp53bp1*$^{-/-}$ mice is reactive to intestinal bacteria, and suggest that IgD responses against commensal bacteria are prominent in the small intestine.

Signals Derived from Gut Microbiota Regulate IgD Production. S_μ-σ_δ CSR is stimulated by both T-cell–dependent and T-cell–independent (TI) immune response pathways (9). We used WT; *Igh*$^{B1\text{-}8+}$ or *Trp53bp1*$^{-/-}$;*Igh*$^{B1\text{-}8+}$ mice to measure antibody responses to immunization. *Igh*$^{B1\text{-}8+}$ transgenic mice express a recombined variable region derived from a 4-hydroxy-3-nitrophenylacetyl (NP) hapten-binding antibody in place of the endogenous 3′ *Igh*-D element (DQ52) and the *Igh*-J elements (15), produce antibodies with high affinity for NP antigens, and thus mount a robust NP-specific Ig response. Immunization of WT;*Igh*$^{B1\text{-}8+}$ or *Trp53bp1*$^{-/-}$;*Igh*$^{B1\text{-}8+}$ mice with NP hapten conjugated to lipopolysaccharide (NP-LPS), a TI type I antigen, elicited similar amounts of NP-specific IgM (requiring no CSR) and reduced amounts of NP-specific IgG (requiring cCSR) in the serum of *Trp53bp1*$^{-/-}$;*Igh*$^{B1\text{-}8+}$ mice compared with levels in WT;*Igh*$^{B1\text{-}8+}$ mice at 14 d after immunization, as expected (Fig. 4*A*). However, serum NP-specific IgD was elevated in *Trp53bp1*$^{-/-}$;*Igh*$^{B1\text{-}8+}$ mice compared with WT;*Igh*$^{B1\text{-}8+}$ mice. Thus, concerning the spontaneous production of IgD in *Trp53bp1*$^{-/-}$ mice, we hypothesized that components of the microbial flora might serve as a driver in a manner similar to immunization. Although *Trp53bp1*$^{-/-}$ mice were not deliberately exposed to exogenous antigens in our specific pathogen-free barrier facility, they began to produce detectable levels of secreted IgD following a latency period (from birth to age 4–6 wk), during which we detected no changes in IgD production. The foregoing observations raised the possibility that endogenous stimulation or environmental antigen exposure during the latency period drives S_μ-σ_δ CSR in B cells of MALT. Thus, we tested whether a signal from the intestinal microbiota contributed to S_μ-σ_δ CSR in *Trp53bp1*$^{-/-}$ mice. Depletion of the microbiota with broad-spectrum antibiotics (Fig. 4*B*) reduced serum IgD levels in *Trp53bp1*$^{-/-}$ mice (Fig. 4*C*).

Next, we used germ-free (GF) mice that were microbiologically sterile and lacked intestinal microbiota. We adoptively transferred WT or *Trp53bp1*$^{-/-}$ BM into conventionally reared (CNV) or GF-*Rag1*$^{-/-}$ mice. As expected, CNV.*Rag1*$^{-/-}$ mice engrafted with *Trp53bp1*$^{-/-}$ BM displayed elevated serum IgD as

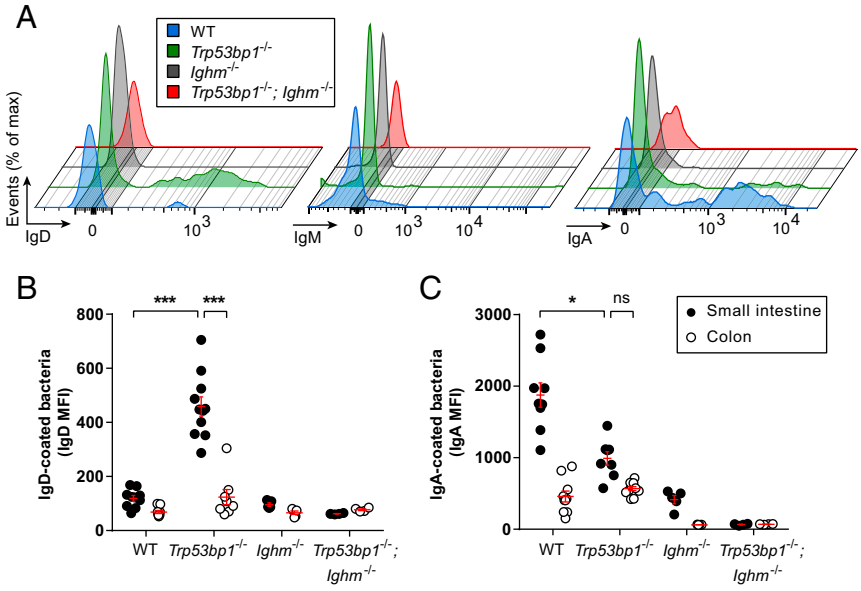

Fig. 3. IgD produced by *Trp53bp1*-deficient B cells recognizes intestinal bacteria. (*A*) Binding of serum IgD, IgM, and IgA to intestinal bacteria. Serum from 12- to 14-wk-old *Trp53bp1*$^{-/-}$, *Ighm*$^{-/-}$, *Trp53bp1*$^{-/-}$;*Ighm*$^{-/-}$, and WT littermates was incubated in vitro with bacteria isolated from the gut of *Ighm*$^{-/-}$ mice. Unbound antibodies were removed by extensive washing, and IgD-bound bacteria were stained and measured by flow cytometry. (*B* and *C*) IgD-coated (*B*) and IgA-coated (*C*) intestinal bacteria from 12- to 14-wk-old indicated mouse strains were analyzed by flow cytometry. Note that *Trp53bp1*$^{-/-}$ mice produce serum IgA at concentrations lower than those in WT mice, but higher than those in *Ighm*$^{-/-}$ mice. Data points represent individual mice. *P* values were determined by Student's *t* test. Results are representative of two independent experiments with $n = 4$–11 mice/genotype or strain. Error bars indicate SD.

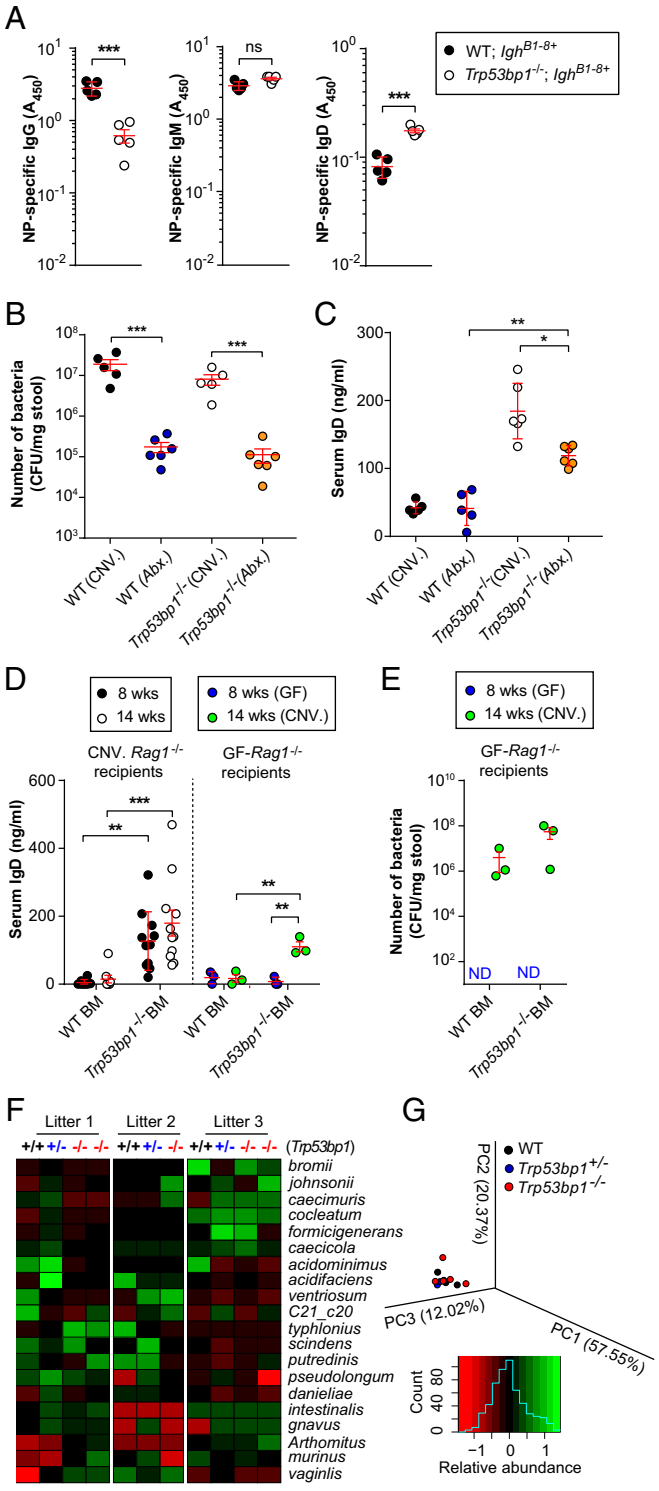

Fig. 4. Hyper-IgD production in *Trp53bp1*$^{-/-}$ mice requires microbiota. (*A*) Serum NP-specific IgG, IgM, and IgD titers measured at 14 d after immunization with NP-LPS. *Igh*$^{B1\text{-}8+}$ transgenic mice express a recombined variable region derived from an NP-binding antibody in place of the endogenous 3′ *Igh*-D element (DQ52) and the *Igh*-J elements (15). (*B* and *E*) Number of bacteria in stool samples freshly isolated from conventionally reared (CNV) mice, broad-spectrum antibiotic-treated (Abx) mice, and GF-*Rag1*$^{-/-}$ recipients. Samples were diluted and plated on BHI blood agar plates. (*C*) Serum IgD concentrations in 10-wk-old CNV and Abx-treated mice of the indicated genotypes. (*D*) Serum IgD concentrations in CNV and GF-*Rag1*$^{-/-}$ recipients before and after microbiota colonization. GF-*Rag1*$^{-/-}$ recipients were colonized with normal intestinal bacteria at 8 wk after BM engraftment. (*F* and *G*) Fecal samples collected from the small intestine of *Trp53bp1*$^{+/-}$ mice, *Trp53bp1*$^{-/-}$ mice, and WT littermates from three independent litters were subjected to 16S rRNA metagenomic sequencing. (*F*) Heat map of fold differences in relative abundance of commensal bacteria. The top 20 commensal genera that differed among the indicated genotypes are presented. (*G*) Principal coordinates analysis plot of fecal microbiota. In *A*–*E*, *P* values were determined by Student's *t* test. Results are representative of two independent experiments with n = 3–11 mice/genotype or strain. Error bars indicate SD.

early as 8 wk after BM engraftment, and the phenotype became more evident over time (Fig. 4*D*). In contrast, GF-*Rag1*$^{-/-}$ mice that received *Trp53bp1*$^{-/-}$ BM showed serum IgD levels comparable to those of CNV.*Rag1*$^{-/-}$ mice reconstituted with WT BM (Fig. 4*D*). After housing these GF-*Rag1*$^{-/-}$ recipients under GF conditions for 8 wk, we then colonized them with normal intestinal bacterial flora (Fig. 4*E*). The conventionalized GF-*Rag1*$^{-/-}$ recipients engrafted with *Trp53bp1*$^{-/-}$ BM showed a significant rise in serum IgD levels compared with conventionalized GF-*Rag1*$^{-/-}$ recipients reconstituted with WT BM (Fig. 4*D*). Taken together, data from the use of gnotobiotic techniques show that signals from intestinal microbiota drive S_μ-σ_δ CSR in *Trp53bp1*$^{-/-}$ mice.

We next used 16S rRNA metagenomic sequencing to examine whether the elevated IgD production in *Trp53bp1*$^{-/-}$ mice is associated with intestinal dysbiosis. The commensal ecology of *Trp53bp1*$^{-/-}$ mice was not markedly different from that of *Trp53bp1*$^{+/-}$ or WT littermates that had been cohoused for their entire lives (Fig. 4*F* and Fig. S5*A*). Principal coordinate analysis performed to visualize the overall microbial community structure showed a similar trend for WT, *Trp53bp1*$^{+/-}$, and *Trp53bp1*$^{-/-}$ mice (Fig. 4*G* and Fig. S5*B*). These results suggest that an altered intestinal microbiome does not cause increased IgD production in *Trp53bp1*$^{-/-}$ mice.

Because microbes are important for driving S_μ-σ_δ CSR, we examined the molecular mechanisms through which microbiota-driven signals elicit hyper-IgD syndrome. Neither B-cell IgD MFI nor serum IgD levels were restored toward WT levels in *Tlr4*$^{Lps3/Lps3}$ and *Ticam1*$^{Lps2/Lps2}$;*Irak4*$^{otiose/otiose}$ hosts reconstituted with BM from *Trp53bp1*$^{-/-}$ donors, indicating that extrahematopoietic TLR signaling is dispensable for the development of hyper-IgD production by *Trp53bp1*$^{-/-}$ B cells (Fig. 5 *A* and *B*). In contrast, a null mutation of MyD88 induced by CRISPR/Cas9 targeting on a *Trp53bp1*$^{-/-}$ background extended the latency period preceding detectable changes in B-cell IgD MFI, reduced the magnitude of the decrease in IgD MFI (Fig. 5*C*), and partially suppressed the serum IgD elevation observed in *Trp53bp1*$^{-/-}$ control mice (Fig. 5*D*). A mutation of *Ticam1* had no effect on these parameters (Fig. 5 *C* and *D*). These data indicate that hyper-IgD syndrome caused by 53BP1 deficiency is partially dependent on hematopoietic-intrinsic MyD88 expression.

Microbiota Control IgD Production in WT NALT B Cells. Because B cells located in human respiratory mucosa generate IgD$^+$IgM$^-$ plasmablasts that secrete IgD into the circulation (9), we focused our attention on B cells in the NALT of WT mice. Specifically, we wished to determine whether S_μ-σ_δ CSR occurs in WT NALT under normal circumstances, and whether this is dependent on the microbiota. We found that NALT B cells produced detectable S_μ-σ_δ junctions (Fig. 2*E*) and presumably were responsible for the serum IgD titers measured in the blood of WT mice (Figs. 1–5), although levels were lower than those seen in *Trp53bp1*$^{-/-}$ mice.

We investigated the requirement for microbiota in S_μ-σ_δ CSR and IgD production by B cells in WT NALT. As expected for GF conditions (16, 17), serum IgE was elevated in GF-WT mice compared with CNV.WT mice, and 53BP1 deficiency suppressed this elevation (Fig. S6), consistent with the absence of cCSR in 53BP1-deficient mice. Flow cytometry analysis of B cells isolated

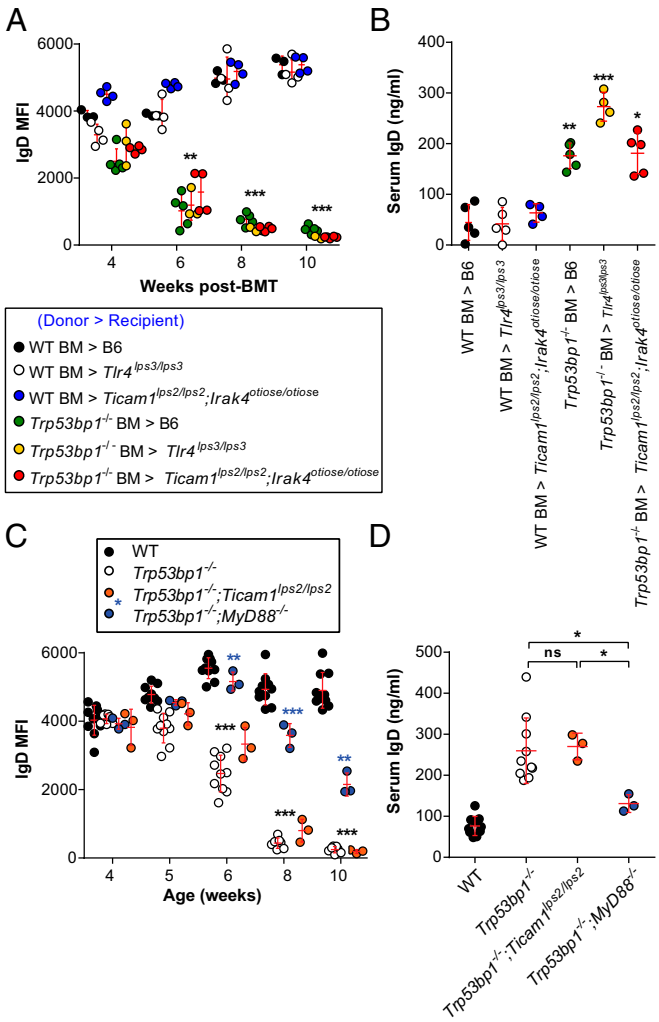

Fig. 5. Hematopoietic-intrinsic MyD88 expression is required for IgD production by *Trp53bp1*$^{-/-}$ B cells. (*A*) IgD MFI on peripheral blood B cells in BM chimeras rescued from lethal irradiation. WT or *Trp53bp1*$^{-/-}$ BM was used to reconstitute WT, *Tlr4*$^{lps3/lps3}$, and *Ticam1*$^{lps2/lps2}$;*Irak4*$^{otiose/otiose}$ mutant recipients. Chimerism was assessed using congenic CD45 markers. All mice used in the experiments demonstrated at least 95% hematopoietic engraftment. Cells were stained in the presence of serum. (*B*) Serum IgD concentration in the indicated chimeric mice at 14 wk after BM transplantation. (*C*) IgD MFI on peripheral blood B cells from mice of the indicated ages and genotypes. Cells were stained in the presence of serum. (*D*) Serum IgD concentration in 10-wk-old mice of the indicated genotypes. *P* values were determined by Student's *t* test and correspond to differences between the marked group and WT recipients for a given time point. In *A*, asterisks for *P* values apply similarly to green, yellow, and red data points. In *C*, black asterisks for *P* values apply similarly to white and orange data points. Data points represent individual mice. Results are representative of two independent experiments with n = 3–10 mice/genotype or strain. Error bars indicate SD.

from the NALT of CNV.WT and GF-WT mice indicated significantly higher frequencies of IgD^{+}IgM^{-} cells (Fig. 6 *A* and *B*), which displayed lower B220 and CD19 expression, in CNV.WT mice compared with GF-WT mice (Fig. 6 *D* and *E*). We confirmed a significant increase in serum IgD in CNV.WT mice with respect to GF-WT mice (Fig. 6*C*). Southern blot analysis of S_{μ}-S_{δ} junctions further confirmed that B cells in NALT of GF-WT mice did not undergo detectable levels of S_{μ}-S_{δ} CSR (Fig. 6*F*); however, conventionalized GF-*Rag1*$^{-/-}$ recipients (ex-GF-*Rag1*$^{-/-}$) engrafted with either WT or *Trp53bp1*$^{-/-}$ BM displayed S_{μ}-S_{δ} CSR in B cells of NALT (Fig. 6*F*). Thus, the development of IgD-producing B cells in NALT of WT mice is microbiota-dependent. We also noted that ex-GF-*Rag1*$^{-/-}$ mice engrafted with *Trp53bp1*$^{-/-}$ BM displayed S_{μ}-S_{δ} CSR in B cells of MLN and SMLN, but those engrafted with WT BM did not (Fig. 6*F*). B cells from MLN and SMLN of conventionally housed germ line *Trp53bp1*$^{-/-}$ mice, but not WT mice, also showed S_{μ}-S_{δ} CSR (Fig. 2*E*).

Discussion

Our findings demonstrate the existence of a previously unrecognized pathway that controls S_{μ}-S_{δ} CSR. Hyperactivation of this pathway in 53BP1-deficient mice may be a compensatory response to the lack of antibody isotypes normally produced by cCSR, and thus may confer a protective effect. Unlike cCSR (5, 18), S_{μ}-S_{δ} CSR is functional in the absence of 53BP1, possibly because 53BP1 may be dispensable for short-range DNA end-joining (11, 12). 53BP1 is known to block DNA end resection and thereby promote NHEJ during cCSR; conversely, intra-switch recombination via HR is favored in the 53BP1-deficient state (13, 19). The mechanistic driver of IgD CSR in the 53BP1-deficient state and in other mutant mice lacking cCSR remains unknown. We noticed that a commonality in 53BP1 and 3′RR deficiency is a failure to support proper synapsis of DSB ends (11, 12, 20), which may permit DNA end resection leading to HR. A corollary is that deficiency of H2AX, another suppressor of DNA end resection (21, 22), might result in a mechanistically similar hyper-IgD phenotype.

Our data suggest that both A-NHEJ and HR pathways contributed to the increased IgD CSR in 53BP1-deficient B cells, with the HR pathway likely making the greater contribution, as suggested by the moderate (~30%) reduction in serum IgD observed on inhibition of A-NHEJ. This is consistent with the known negative regulatory effect of DNA end resections generated during HR toward ATM, on which A-NHEJ is dependent. Importantly, our findings establish that short-range interswitch S_{μ}-S_{δ} CSR can be robustly supported by HR.

We have shown that S_{μ}-S_{δ} CSR is activated in response to commensal microbial stimuli. S_{μ}-S_{δ} CSR has been observed in B cells of mouse MLNs and human tonsils, consistent with our observation that S_{μ}-S_{δ} CSR was confined to MALT in WT mice and to NALT and MLN/SMLN in 53BP1-deficient mice. The reduced levels of microbiota-derived antigens likely present in the MLNs/SMLNs compared with the NALT itself may result in the occurrence of IgD CSR events at a number below the level of detection in WT mice, whereas exaggerated IgD CSR induced by the same number of antigens may result in detectable levels of S_{μ}-S_{δ} junctions in *Trp53bp1*$^{-/-}$ mice. Importantly, we have shown that S_{μ}-S_{δ} CSR is activated in response to at least one innate sensing pathway that detects commensal microbes, i.e., Toll-like receptor (TLR) signaling.

The nature of the molecular signature that activates TLR-dependent S_{μ}-S_{δ} CSR remains to be determined, as does the mechanism by which signaling from MyD88 promotes S_{μ}-S_{δ} CSR. We noted that nonhematopoietic TLR4 deficiency exacerbated the serum IgD elevation resulting from *Trp53bp1*$^{-/-}$ BM transfer, an interesting finding in light of the hyper-IgD syndrome caused by MvK deficiency, in which TLR4-dependent proinflammatory cytokine secretion was elevated in an IL-1 receptor-dependent manner (23). Apparently, there may be a link between aberrant TLR4 signaling (too high or too low) and hyper-IgD that remains to be explored.

Secreted IgD has been reported to bind specifically to basophils and activate basophil production of B-cell–activating factors, antimicrobial factors, and proinflammatory cytokines—functions that may be dysregulated in autoimmune disease (9). We postulate that secreted IgD may have separate duties in the recognition of commensal microbial flora, and may contribute to the homeostatic regulation of the microbial community, insofar as its production via CSR is dependent on signals from the microbiome.

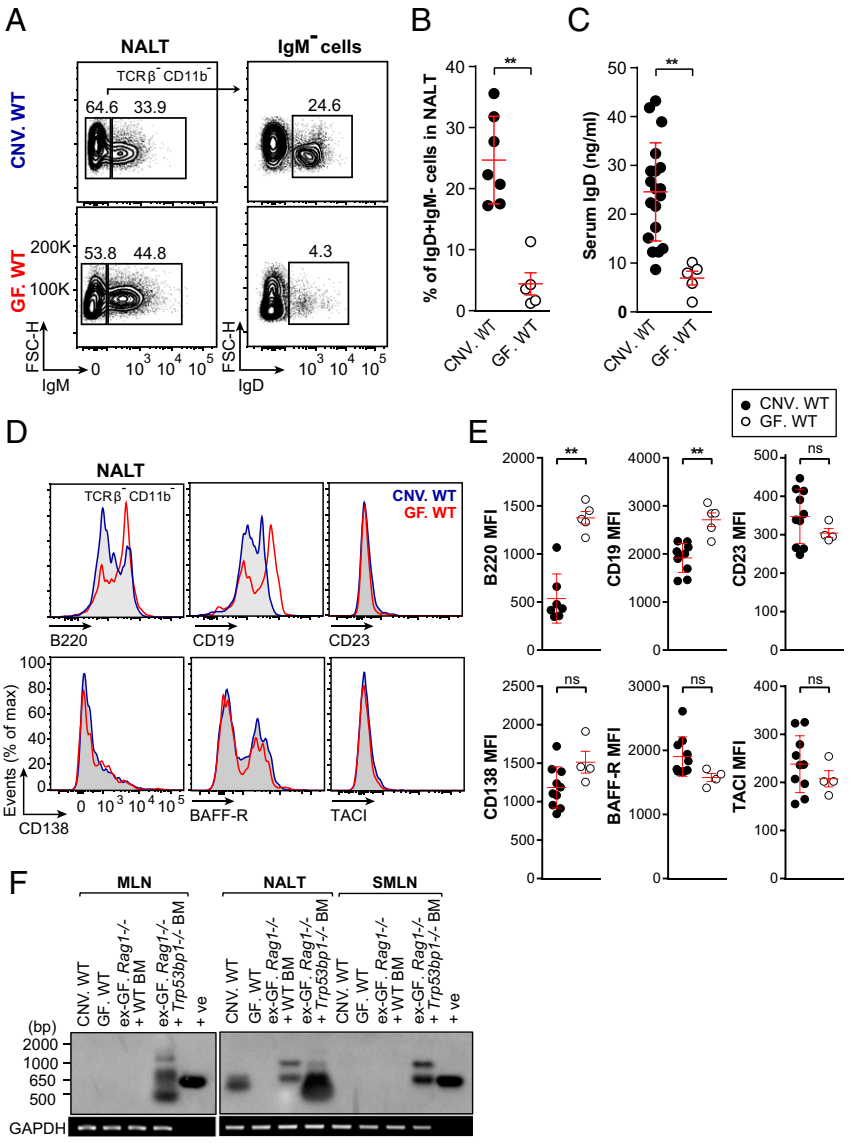

Fig. 6. Requirement for microbiota in IgD-secreting B-cell development. (*A*) Representative flow cytometry analysis of IgD$^+$IgM$^-$ cells in NALT of CNV and GF C57BL/6J mice. Cells were gated first on IgM$^-$ cells and then on IgD$^+$ cells. The percentage of cells in each gate is indicated. (*B*) Percentage of IgD$^+$IgM$^-$ B cells isolated from NALT. (*C*) Serum IgD concentration in 12-wk-old mice. (*D* and *E*) Flow cytometry analysis of B220, CD19, CD23, CD138, BAFF-R, and TACI expression on IgD$^+$IgM$^-$ B cells from NALT of CNV and GF WT mice. Representative FACS plots are shown in (*D*). (*F*) GF-*Rag1*$^{-/-}$ mice were engrafted with *Trp53bp1*$^{-/-}$ or WT BM and 8 wk later colonized with normal intestinal bacteria; they were then conventionally housed for 5 mo (ex-GF-*Rag1*$^{-/-}$ plus indicated BM). Southern blot analysis of S_μ-σ_δ junctions in B cells from MLNs, NALT, and SMLNs of the indicated mice. Data points represent individual mice (*B*, *C*, *E*). *P* values were determined by Student's *t* test. Results are representative of three independent experiments with $n = 3$–14 mice/genotype or strain. Error bars indicate SEM.

Materials and Methods

Mice. Eight- to 10-wk-old pure C57BL/6J background males purchased from The Jackson Laboratory were mutagenized with ENU as described previously (24). Mutagenized G0 males were bred to C57BL/6J females, and the resulting G1 males were crossed to C57BL/6J females to produce G2 mice. G2 females were backcrossed to their G1 sires to yield G3 mice, which were screened for phenotypes. Whole-exome sequencing and mapping were performed as described previously (4).

Rag1$^{-/-}$, *Rag2*$^{-/-}$, *Ighm*$^{-/-}$, *Atm*$^{-/-}$, and *Igh*^{tm2Cgn} (*Igh*$^{B1\text{-}8}$) transgenic mice were purchased from The Jackson Laboratory. *Tlr4*$^{lps3/lps3}$, *Ticam1*$^{lps2/lps2}$, *Irak4*$^{otiose/otiose}$, *CD40*$^{bluebonnet/bluebonnet}$, *Tnfsf13b*$^{frozen/frozen}$, and *Dock8*$^{snowdrop/snowdrop}$ strains were generated by ENU mutagenesis as described online (mutagenetix.utsouthwestern.edu), and are available from the Mutant Mouse Regional Resource Center. *Trp53bp1*$^{-/-}$;*Rag2*$^{-/-}$, *Trp53bp1*$^{-/-}$;*Ighm*$^{-/-}$, *Trp53bp1*$^{-/-}$;*Igh*$^{B1\text{-}8}$, *Trp53bp1*$^{-/-}$*Atm*$^{-/-}$, *Trp53bp1*$^{-/-}$ *Ticam1*$^{lps2/lps2}$, and *Ticam1*$^{lps2/lps2}$;*Irak4*$^{otiose/otiose}$ mice were generated by intercrossing mouse strains.

Germ-free C57BL/6 and *Rag1*$^{-/-}$ mice were provided by the University of Texas Southwestern Medical Center's Gnotobiotic Mouse Facility. Conventionally reared mice were housed in specific pathogen-free conditions at the University of Texas Southwestern Medical Center, and all experimental procedures were performed in accordance with institutionally approved protocols.

Generation of Knockout Mouse Strains Using the CRISPR/Cas9 System. To generate single knockout mouse strains, female C57BL/6J mice were superovulated by injection of 6.5 U of pregnant mare serum gonadotropin (EMD Millipore), followed by injection of 6.5 U of human chorionic gonadotropin (Sigma-Aldrich) 48 h later. The superovulated mice were subsequently mated overnight with C57BL/6J male mice. The next day, fertilized eggs were collected from the oviducts, and in vitro-transcribed Cas9 mRNA (50 ng/μL) and Trp53bp1 or Pla2g4b small base-pairing guide RNA (50 ng/μL; Trp53bp1: 5′-TTTGACCAGAGTAGTAAAACAGG-3′; Pla2g4b: 5′-GGCACTGGCCAACCTC-TATGAGG-3′) were injected into the cytoplasm or pronucleus of the

embryos. For the generation of double-knockout strains (*Trp53bp1*$^{-/-}$; *Aicda*$^{-/-}$, *Trp53bp1*$^{-/-}$;*MyD88*$^{-/-}$), Aicda or MyD88 small base-pairing guide RNA (50 ng/μL; Aicda: 5′-CGGTGAAAATCCTCAGGCTGAGG-3′; MyD88: 5′-GCTCCTTCAGTATATCCTCACGG-3′) and in vitro-transcribed Cas9 mRNA were injected into the *Trp53bp1*$^{-/-}$ embryos. The injected embryos were cultured in M16 medium (Sigma-Aldrich) at 37 °C in 5% CO_2. For the production of mutant mice, two-cell stage embryos were transferred into the ampulla of the oviduct (10–20 embryos per oviduct) of pseudopregnant Hsd:ICR (CD-1) female mice (Harlan Laboratories).

BM Chimeras. Recipient mice were lethally irradiated with 9 Gy (*Trp53bp1*$^{-/-}$ mice) or 15 Gy (WT mice) via gamma radiation (X-RAD 320; Precision X-Ray). The mice then received i.v. injections of 5×10^6 BM cells derived from the tibia and femurs of the respective donors. The mice were maintained on an antibiotic regimen for 4 wk after BM engraftment. Starting at 4 wk after engraftment, the chimeras were bled biweekly to assess surface IgD expression by FACS. Chimerism was assessed using congenic CD45 markers. At 14 wk after engraftment, the chimeras were bled to assess serum IgD levels by ELISA.

Antibiotic Treatment. Mice were given autoclaved water with or without ampicillin (1 mg/mL), vancomycin (500 μg/mL), neomycin (1 mg/mL), metronidazole (1 mg/mL), and streptomycin (1 mg/mL) continuously by ad libitum administration in drinking water for the duration of the experiment (up to 7 wk). All antibiotics were obtained from Sigma-Aldrich. Microbiota depletion was confirmed by culture of intestinal contents on brain-heart infusion (BHI) agar (Sigma-Aldrich) containing 10% (vol/vol) calf blood.

Germ-Free Mouse Experiments. Freshly isolated BM cells from 8-wk-old *Trp53bp1*$^{-/-}$ and WT littermates were transferred i.v. into 12-wk-old GV-*Rag1*$^{-/-}$ and CNV.*Rag1*$^{-/-}$ recipients (2×10^7 cells/mouse). The recipients were housed in either GF or conventional mouse facilities for 8 wk. The recipients were bled biweekly starting at 4 wk after BM engraftment. At 8 wk after BM adoptive transfer, the GF-*Rag1*$^{-/-}$ recipients were colonized with a normal intestinal bacterial flora by spreading fecal contents from WT mice on their fur, followed by housing them with conventionally reared mice. Bacterial loads in conventionalized GF mice were assessed by plating mouse fecal contents on BHI blood agar plates.

Flow Cytometry. BM cells, splenocytes, and peritoneal cavity cells were isolated, and red blood cell (RBC) lysis buffer was added to remove the RBCs. Cells were stained at 1:200 dilution with mouse fluorochrome-conjugated monoclonal antibodies specific for murine cell surface markers CD3, B220, CD21, CD23, and IgM (BD Pharmingen); IgD (Biolegend); and CD19 and CD93 (eBiosicence) and in the presence of anti-mouse CD16/32 antibody (Tonbo Biosciences) for 1 h at 4 °C.

For detection of surface IgD expression on peripheral blood B cells, 100 μL of blood was stained with an antibody mixture containing equal volumes of CD3, B220, IgM, IgD, CD45.1, CD45.2, and CD16/32 antibodies (1:200 dilution) in the presence of serum for 1 h at 4 °C. After RBC lysis, cells were washed and analyzed by FACS. In addition, an equal volume of blood was subjected to RBC lysis, and remaining cells were washed three times in ice-cold PBS to remove serum. The cells were then stained with the same antibody mixture under the same conditions.

For the serum replacement experiment, 100 μL of WT blood cells were spun at $1,500 \times g$ for 5 min, and 50 μL of serum was removed by pipette. Then 50 μL of freshly isolated serum from *Trp53bp1*$^{-/-}$, *Trp53bp1*$^{-/-}$;*Rag2*$^{-/-}$, *Trp53bp1*$^{-/-}$;*Ighm*$^{-/-}$, or WT littermates was added to the WT blood pellet. The pellet was resuspended and then incubated for 2 h at 37 °C. Then the antibody mixture was added to the serum-replaced WT blood, followed by another 1-h incubation at 4 °C. After staining, RBCs were lysed, remaining cells were washed, and surface IgD expression was analyzed by FACS. Data were acquired on an LSRFortessa cell analyzer (BD Bioscience) and analyzed with FlowJo software (Tree Star).

For detection of antibody-coated bacteria by flow cytometry, 10 mg of fecal contents isolated from *Ighm*$^{-/-}$ mice was suspended in 100 μL of sterile PBS, homogenized, and centrifuged twice at $600 \times g$ for 5 min to remove large particles in the feces. Cleared supernatants were centrifuged at $9,000 \times g$ for 5 min to pellet bacteria. The pellet was resuspended in freshly isolated serum from *Trp53bp1*$^{-/-}$, *Ighm*$^{-/-}$, *Trp53bp1*$^{-/-}$;*Ighm*$^{-/-}$, and WT littermates for 2 h at 37 °C. Then the bacteria were washed extensively three times with sterile PBS to remove nonbound immunoglobulins. The bacteria pellets were stained with a fluorescent-labeled antibody mixture containing equal volumes of IgD, IgM, and IgA antibodies for 45 min at 4 °C, then washed and resuspended in 2.5 μg/mL DAPI in PBS. All events stained with DAPI were considered bacteria. Measurements were performed with an LSRFortessa cell analyzer (BD Bioscience) using forward scatter and side scatter thresholds set at the minimum possible setting of 200, with a slow flow rate.

Immunization. B-cell receptor transgenic mice (WT;*Igh*$^{B1\text{-}8}$ or *Trp53bp1*$^{-/-}$;*Igh*$^{B1\text{-}8}$) were immunized i.p. with NP-LPS (50 μg; Biosearch Technologies) on day 0 as described previously (25). At 14 d after immunization, blood was collected in MiniCollect Tubes (Mercedes Medical) and centrifuged at $1,500 \times g$ to separate the serum.

For ELISA analysis of antigen-specific IgM and IgG responses, Nunc MaxiSorp flat-bottom 96-well microplates (Thermo Fisher Scientific) were coated with 5 μg/mL NP_8-BSA (Biosearch Technologies) at 4 °C overnight. The plates were then washed four times with washing buffer [0.05% (vol/vol) Tween-20 in PBS] using a BioTek microplate washer, then blocked with 1% (vol/vol) BSA for 1 h at room temperature. Serum samples were serially diluted in 1% (vol/vol) BSA, after which the 1:50 and 1:150 dilutions were added to the prepared ELISA plates. After a 2-h incubation, the plates were washed eight times with washing buffer and then incubated with HRP-conjugated goat anti-mouse IgM or IgG for 1 h at room temperature. The plates were washed eight more times with washing buffer, and then developed with SureBlue TMB Microwell Peroxidase Substrate and TMB Stop Solution (KPL). Absorbance was measured at 450 nm on a Synergy Neo2 Plate Reader (BioTek). Basal levels of anti-NP IgG and IgM were determined using preimmune serum. The antigen-specific IgG and IgM were determined as the OD value postimmunization minus the OD value before immunization for each individual mouse. All ELISA data shown represent the 1:150 serum dilution.

Antigen-specific serum IgD level was measured on NP_8-BSA–coated 96-well microplates. Diluted serum (1:2 dilution in 1% BSA) was added, followed by a 2-h incubation. After washing, plates were incubated with biotinylated anti-mouse IgD, followed by incubation with streptavidin-conjugated HRP. Plates were developed, and the antigen-specific IgD was determined as described above.

For determination of serum antibody isotype levels, freshly isolated serum was subjected to sandwich ELISA analysis according to the manufacturer's instructions (eBiocience; MyBioSource).

Southern Blot Analysis of S_μ-σ_δ Junctions. B cells in BM, spleen, MLNs, bronchoalveolar lavage fluid, NALT, and SMLNs were negatively enriched using the mouse Pan B-Cell Isolation Kit (Miltenyi Biotech). Genomic DNA was extracted from isolated B cells using the QIAamp DNA Mini Kit (Qiagen) according to the manufacturer's instructions. S_μ-σ_δ junctions were amplified using touchdown PCR, followed by nested PCR using primers targeting the 5′ S_μ and 3′ C_δ, as described previously (1). Primers for touchdown PCR were 5′-CAGTTGAGGCCAGCAGGT-3′ and 5′-CCAATTACTAAACAGCCCAGGT-3′ (one cycle at 98 °C for 3 min; three cycles at 98 °C for 30 s, 64 °C for 40 s, and 72 °C for 90 s; three cycles at 98 °C for 30 s, 62 °C for 40 s, and 72 °C for 90 s; 25 cycles at 98 °C for 30 s, 60 °C for 40 s, and 72 °C for 90 s; and one cycle at 72 °C for 7 min), and primers for nested PCR were 5′-CAGGTCGGCTGGACTAACTC-3′ and 5′-CAGCCCAGGTTTATCTTTTCA-3′ (one cycle at 98 °C for 3 min; 35 cycles at 98 °C for 30 s, 65 °C for 40 s, and 72 °C for 90 s; and one cycle at 72 °C for 7 min). Hybridization of S_μ-σ_δ junctions was performed with a biotinylated probe (460 bp), which was cloned as a PCR fragment from the intron 5′ to C_δ (5′-CCCAGAACCTGAGAAGGAAG-3′) and the C_δ exon (5′-CAGCCCAGGTTTATCTTTTCA-3′). The probe was biotinylated using the Detector PCR DNA Biotinylation Kit (KPL). The probe hybridized to S_μ-σ_δ junctions was visualized with the Detector HRP Chemiluminescent Blotting Kit (KPL) according to the manufacturer's instructions. A PCR-amplified fragment encompassing the 460-bp probe sequence served as the positive control for the assay.

Quantitative RT-PCR Analysis for I_μ-C_μ and I_μ-C_δ Transcripts. Total RNA was isolated from BM, spleen, and blood using TRIzol Reagent (Thermo Fisher Scientific) according to the manufacturer's instructions. DNase treatment and cleanup were performed using the DNA-free DNase Treatment and Removal Reagents Kit (Thermo Fisher Scientific). Here 1 μg of RNA was reverse-transcribed to cDNA with SuperScript III First-Strand Synthesis System for RT-PCR (Life Technologies). Transcript levels of Iμ-Cμ (membrane Cμ) and Iμ-Cδ were analyzed using iTaq Universal SYBR Green Supermix (Bio-Rad) on a Step One Plus Real-Time PCR System (Life Technologies) with the following primers as described previously (1): Iμ-Cμ: 5′-TGGAACTCCGGAGAGACCTA-3′ and 5′-TTCCTCCTCAGCATTCACCT-3′; Iμ-Cδ: 5′-CTCTGGCCCTGCTTATTGTTG-3′ and 5′-GCTCCCAGCTGATTTTCAGT-3′. Relative expression was calculated with the ΔΔCt standardization method using *Pax5* primers (5′-CGAGTCTGTGACAATGACACTGTGC-3′ and 5′-CAGGATGCCACTGATGGAGTATG-3′).

16S rRNA Metagenomics Analysis. Stool samples from small intestine and colon of *Trp53bp1*$^{-/-}$ mice and their heterozygous or WT littermates that were cohoused for their entire life were collected, and bacterial DNA was extracted using the following protocol. Stool samples were suspended in ice-cold PBS and briefly centrifuged to remove large fecal contents. Lysozyme (5 mg/mL) was added to the cleared supernatants, followed by incubation for 30 min at 37 °C. The solution was transferred to Lysing Matrix bead tubes (0.1-mm glass beads; MP Biomedical), and the beads were vortexed (1 min at top speed, 2 min on ice) five times to ensure efficient lysis of bacteria. The tubes were then spun for 1 min at 16,000 × *g* for 2 min, after which the supernatant was transferred to a sterile 2-mL microfuge tube. An equal volume of phenol/chloroform/isoamyl alcohol was added to the tube, followed by vigorous shaking for 10 s. The samples were centrifuged at 16,000 × *g* for 2 min, after which the aqueous phase was transferred to a clean microfuge tube and extracted with an equal volume of chloroform. The samples were then centrifuged again at 16,000 × *g* for 2 min, after which the chloroform extraction was repeated. The aqueous phase was transferred to a clean microfuge tube, and the nucleic acids were precipitated by the addition of 0.3 M sodium acetate (pH 7.0) and 2.5 volumes of isopropanol. The samples were incubated at −20 °C for 2 h, followed by centrifugation at 16,000 × *g* for 30 min. The precipitated nucleic acid was washed once with 700 μL of 70% ethanol and centrifuged at 16,000 × *g* for 10 min. The supernatant was decanted, and the pellets were allowed to dry at room temperature for 10 min. The nucleic acid was resuspended in nuclease-free water and cleaned over a MinElute spin column (Qiagen).

Next, 50 ng of purified DNA was prepared using an Ion 16S Metagenomics Kit (Thermo Fisher Scientific) according to the manufacturer's instructions. In brief, PCR-amplified hypervariable regions of the 16S region of bacteria were quantified using the Quant-iT PicoGreen Assay (Invitrogen) and normalized. Samples were sequenced on an Ion PGM System (Thermo Fisher Scientific) according to the manufacturer's instructions, and the results were analyzed with the Ion Reporter software Ion 16S Metagenomics Kit analyses module (Thermo Fisher Scientific). Relative proportions of microbial taxa for each sample and the signal-to-noise ratio were assembled as described previously after filtering out singletons (taxa found in only one sample) and low-coverage taxa (those with <20 total reads) (26). Ssignal-to-noise ratios are depicted in heat map plots generated with R software and principal component analyses generated with Ion Reporter software.

Statistical Analysis. The statistical significance of differences between groups was analyzed using GraphPad Prism to perform the indicated statistical tests. Differences in the raw values among groups were considered statistically significant when $P < 0.05$. *P* values are denoted as follows: $*P < 0.05$; $**P < 0.01$; $***P < 0.001$; ns, not significant with $P > 0.05$.

ACKNOWLEDGMENTS. This work was supported by National Institutes of Health Grants U19 AI100627 and R37 GM067759.

1. Rouaud P, et al. (2014) Elucidation of the enigmatic IgD class-switch recombination via germline deletion of the IgH 3′ regulatory region. *J Exp Med* 211(5):975–985.
2. Lutz C, et al. (1998) IgD can largely substitute for loss of IgM function in B cells. *Nature* 393(6687):797–801.
3. Roes J, Rajewsky K (1993) Immunoglobulin D (IgD)-deficient mice reveal an auxiliary receptor function for IgD in antigen-mediated recruitment of B cells. *J Exp Med* 177(1):45–55.
4. Wang T, et al. (2015) Real-time resolution of point mutations that cause phenovariance in mice. *Proc Natl Acad Sci USA* 112(5):E440–E449.
5. Manis JP, et al. (2004) 53BP1 links DNA damage-response pathways to immunoglobulin heavy chain class-switch recombination. *Nat Immunol* 5(5):481–487.
6. Drenth JP, et al.; International Hyper-IgD Study Group (1999) Mutations in the gene encoding mevalonate kinase cause hyper-IgD and periodic fever syndrome. *Nat Genet* 22(2):178–181.
7. Hager EJ, et al. (2007) Deletion of a single mevalonate kinase (Mvk) allele yields a murine model of hyper-IgD syndrome. *J Inherit Metab Dis* 30(6):888–895.
8. Saintamand A, Lecron JC, Morel F, Cogné M, Denizot Y (2015) Comment on "IgH chain class switch recombination: mechanism and regulation". *J Immunol* 194(5):2039–2040.
9. Chen K, et al. (2009) Immunoglobulin D enhances immune surveillance by activating antimicrobial, proinflammatory and B cell-stimulating programs in basophils. *Nat Immunol* 10(8):889–898.
10. Bothmer A, et al. (2011) Regulation of DNA end joining, resection, and immunoglobulin class switch recombination by 53BP1. *Mol Cell* 42(3):319–329.
11. Bothmer A, et al. (2010) 53BP1 regulates DNA resection and the choice between classical and alternative end joining during class switch recombination. *J Exp Med* 207(4):855–865.
12. Difilippantonio S, et al. (2008) 53BP1 facilitates long-range DNA end-joining during V(D)J recombination. *Nature* 456(7221):529–533.
13. Yamane A, et al. (2013) RPA accumulation during class switch recombination represents 5′-3′ DNA-end resection during the S-G2/M phase of the cell cycle. *Cell Reports* 3(1):138–147.
14. Shiotani B, Zou L (2009) Single-stranded DNA orchestrates an ATM-to-ATR switch at DNA breaks. *Mol Cell* 33(5):547–558.
15. Shih TA, Roederer M, Nussenzweig MC (2002) Role of antigen receptor affinity in T cell-independent antibody responses in vivo. *Nat Immunol* 3(4):399–406.
16. Cahenzli J, Köller Y, Wyss M, Geuking MB, McCoy KD (2013) Intestinal microbial diversity during early-life colonization shapes long-term IgE levels. *Cell Host Microbe* 14(5):559–570.
17. Hill DA, et al. (2012) Commensal bacteria-derived signals regulate basophil hematopoiesis and allergic inflammation. *Nat Med* 18(4):538–546.
18. Ward IM, et al. (2004) 53BP1 is required for class switch recombination. *J Cell Biol* 165(4):459–464.
19. Reina-San-Martin B, Chen J, Nussenzweig A, Nussenzweig MC (2007) Enhanced intra-switch region recombination during immunoglobulin class switch recombination in 53BP1$^{-/-}$ B cells. *Eur J Immunol* 37(1):235–239.
20. Saintamand A, et al. (2015) Elucidation of IgH 3′ region regulatory role during class switch recombination via germline deletion. *Nat Commun* 6:7084.
21. Reina-San-Martin B, et al. (2003) H2AX is required for recombination between immunoglobulin switch regions but not for intra-switch region recombination or somatic hypermutation. *J Exp Med* 197(12):1767–1778.
22. Helmink BA, et al. (2011) H2AX prevents CtIP-mediated DNA end resection and aberrant repair in G1-phase lymphocytes. *Nature* 469(7329):245–249.
23. Stoffels M, et al. (2015) TLR2/TLR4-dependent exaggerated cytokine production in hyperimmunoglobulinaemia D and periodic fever syndrome. *Rheumatology (Oxford)* 54(2):363–368.
24. Georgel P, Du X, Hoebe K, Beutler B (2008) ENU mutagenesis in mice. *Methods Mol Biol* 415:1–16.
25. Arnold CN, et al. (2012) A forward genetic screen reveals roles for Nfkbid, Zeb1, and Ruvbl2 in humoral immunity. *Proc Natl Acad Sci USA* 109(31):12286–12293.
26. Lukens JR, et al. (2014) Dietary modulation of the microbiome affects autoinflammatory disease. *Nature* 516(7530):246–249.